[1] **Heena Parveen**

[2] **Dr. A. Raghu Ram**

Grid-Connected hybrid Solar-Wind System with Virtual Synchronous Generator-controlled inverter

Journal of Electrical Systems

Abstract: - This paper presents an inverter based on Virtual Synchronous Generator (VSG) control for a grid-connected hybrid solar-wind system (HSWS). A high-gain SEPIC converter is employed to regulate the output voltage produced by the HSWS. To maximize power extraction from the HSWS, an incremental conductance MPPT control technique is utilized. The system incorporates an inverter that converts the boosted DC voltage to AC, ensuring it meets grid specifications and load requirements. The inverter's output is regulated by a distinctive VSG controller, which emulates the behavior of synchronous generators (SGs), thereby enhancing grid stability and compatibility. A simulation model is developed in MATLAB/Simulink to implement the VSG, ensuring voltage stability and balanced grid frequency even under unbalanced load conditions. The simulation results also demonstrate that using the VSG reduces total harmonic distortion (THD) compared to other systems.

Keywords: Solar System, Wind system, High gain modified SEPIC converter, Incremental conductance MPPT technique, Inverter, Virtual Synchronous generator control, Grid.

I. INTRODUCTION

The integration and utilization of clean energy sources are in high demand, driving significant research in this area. This includes sources like photovoltaic (PV) systems, wind energy, and other renewable energy sources [1], [2].

The power generated by renewable energy sources is used in various industrial applications, but it cannot be directly supplied to the load because the power generation occurs at one voltage level while the load requires a different voltage level. To address this, high-voltage gain DC-DC converters [3] are used. In this paper, a two-switch enhanced gain modified SEPIC converter (TSEGS) is utilized for this purpose [4], [5].

The power generated by renewable sources is not consistent because it depends on weather conditions. However, they should operate at their rated power. For this reason, an MPPT controller [6] is implemented using a DC/DC converter. In this work, the incremental conductance (INC) MPPT technique [7] is used because of its fast and accurate tracking.

An inverter is an essential part of a renewable energy power conversion system, responsible for converting DC to AC to meet the requirements of the grid or loads. Effective control of the inverter is crucial; in this study, the VSG control method [8] is employed to manage the inverter output and synchronize it with the grid.

VSG technology, inspired by synchronous generators (SGs), enables grid-connected renewable energy system (RES) inverters to mimic the dynamic behavior of SGs. By addressing the issues of low inertia and inadequate damping in RES inverters, VSG technology helps create a more resilient and thriving renewable energy future [9].

The power generated by renewable sources is variable. Utilizing a battery bank enhances the system's continuity and reliability [10], [11].

The primary contribution of this work is as follows:

- To design an integrated solar and wind system for power generation and supply to the grid.
- To design a high-gain TSEGS DC-DC converter and an MPPT controller to regulate the DC output voltage and maximize power extraction from the system.
- To develop a VSG control for an inverter to maintain voltage and frequency stability and manage system dynamics in response to varying input and load conditions.

[1] *Jawaharlal Nehru Technological University, Hyderabad, India

[2] Jawaharlal Nehru Technological University, Hyderabad, India

The structure of the paper is as follows: Section II presents the main block diagram of the proposed model and the control techniques employed. Sections III and IV provide a discussion and the simulation results. Section V concludes with the findings of the proposed system.

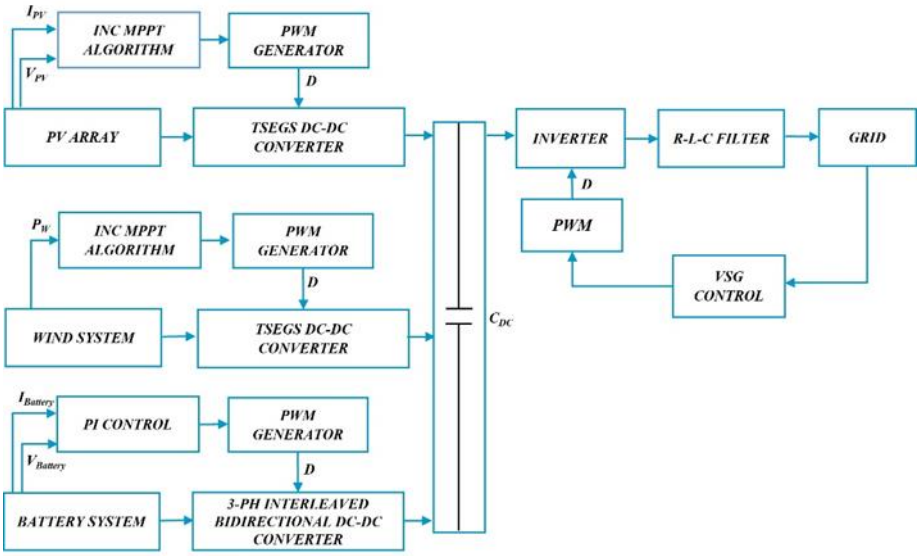

Fig. 1 System Layout

II. DESIGNED CIRCUIT

Fig. 1 illustrates the block diagram of the proposed system, which includes a solar system, a wind system, a battery bank, an inverter with VSG control, and a three-phase grid.

A. Modelling of Solar System

The solar cell is the primary component of the solar system, responsible for converting solar energy into electrical energy. The V-I characteristics of the solar cell is given by (1).

$$I=I_{PV}-I_D-I_{sh} \tag{1}$$

$$I_D=I_o\left[e^{\frac{q(V+IR_S)}{nKN_ST}}-1\right] \tag{2}$$

$$V_t=\frac{KN_ST}{q} \tag{3}$$

$$I_o=I_{rs}\left[\frac{T}{T_n}\right]^3\left[e^{\frac{qE_g\left[\frac{1}{T_n}-\frac{1}{T}\right]}{nK}}\right] \tag{4}$$

$$I_{PV}=[I_{sc}+K_i(T-298)]\frac{G}{G_O} \tag{5}$$

$$I_{sh}=\frac{V+IR_S}{R_{sh}} \tag{6}$$

$$I_{sc}=I_{rs}\left[e^{\frac{qV_{oc}}{nKN_ST}}-1\right] \tag{7}$$

$$I=I_{rs}\left[e^{\frac{qV_{oc}}{nKN_ST}}-1\right]+K_i(T-298)]\frac{G}{G_O}-I_{rs}\left[\frac{T}{T_n}\right]^3\left[e^{\frac{qE_g\left[\frac{1}{T_n}-\frac{1}{T}\right]}{nK}}\right]\left[e^{\frac{q(V+IR_S)}{nKN_ST}}-1\right]-\left[\frac{V+IR_S}{R_{sh}}\right] \tag{8}$$

B. Modelling of wind system

The wind turbine transforms the wind's kinetic energy into mechanical energy, as indicated by (9).

$$P_m = \frac{1}{2} * C_p(\lambda, \beta) * \rho * A * V_w^3 \tag{9}$$

$$C_p = 0.5\left(\frac{116}{\lambda_i} - 0.4\beta - 5\right)e^{\left(\frac{-21}{\lambda_i}\right)} + 0.0068\lambda \tag{10}$$

$$\frac{1}{\lambda_i} = \frac{1}{\lambda + 0.08\beta} - \frac{0.035}{\beta^3 + 1} \tag{11}$$

$$\lambda = \frac{\omega R}{V_w} \tag{12}$$

$$T_m = \frac{P_m}{\omega} = \frac{\frac{1}{2} * C_p(\lambda, \beta) * \rho * A * V_w^3}{\omega} \tag{13}$$

C . Design of TSEGS DC-DC Converter

The TSEGS Converter, depicted in Fig. 2, is utilized to align the HSWS output with the load. The design equations for the converter are provided in equations (14) to (19).

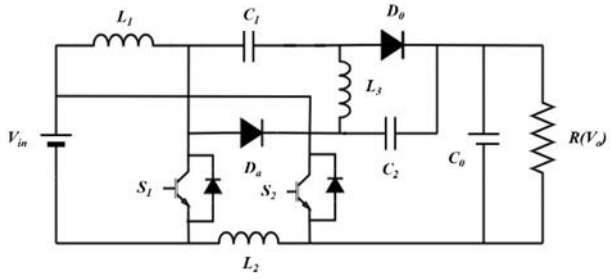

Fig. 2 DC-DC converter

$$L_1 \geq \frac{DV_{in}}{\Delta i_{L1} f_s} \tag{14}$$

$$L_2 \geq \frac{DV_{in}}{\Delta i_{L2} f_s} \tag{15}$$

$$L_3 \geq \frac{2DV_{in}}{\Delta i_{L3} f_s} \tag{16}$$

$$C_1 = \frac{I_0}{\Delta V_{C1} f_s} \tag{17}$$

$$C_2 = \frac{I_0}{\Delta V_{C2} f_s} \tag{18}$$

$$C_o = \frac{2DI_0}{\Delta V_{CO} f_s} \tag{19}$$

The nominal duty cycle (D) and gain (M) of the converter are calculated by (20)-(21).

$$D=\frac{V_o-V_{in}}{V_o+3V_{in}} \tag{20}$$

$$M=\frac{V_o}{V_{in}}=\frac{1+3D}{1-D} \tag{21}$$

D. *Incremental Conductance MPPT Control Scheme*

Incremental Conductance MPPT has been selected for Maximum Power Point Tracking (MPPT) due to its low complexity and ease of implementation. Incremental Conductance MPPT continuously monitors the power and voltage characteristics of the system, adjusting the operating points to maximize power extraction from both solar and wind sources. It accomplishes this by evaluating the conductance (I/V) and the rate of change of conductance (dI/dV). By examining the relationship between these values, the algorithm determines the optimal operating point for the PV and wind system as shown in Fig. 3.

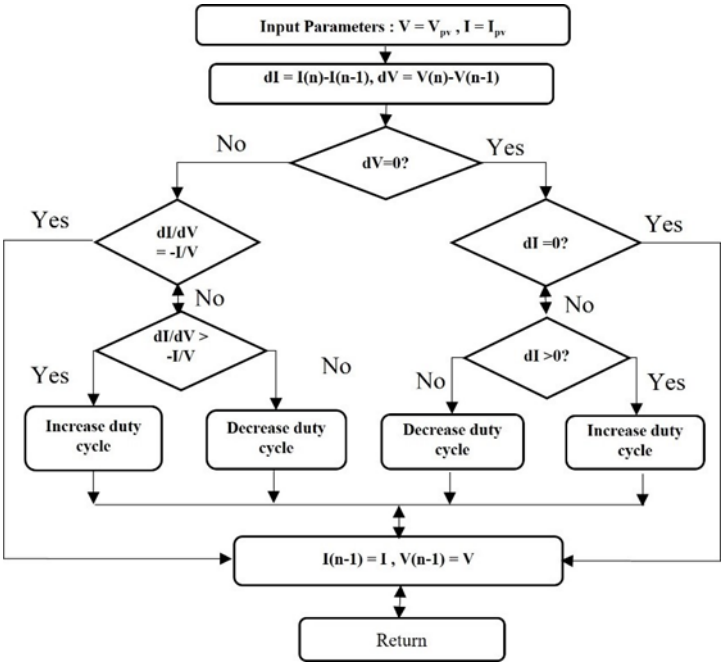

Fig. 3 Flowchart of an INC MPPT control technique

E. Design of Battery System

Fig. 4 shows a schematic of a battery bank connected with a three-phase interleaved bidirectional DC-DC buck-boost converter, which is used to stabilize the DC-link voltage [12], [13]. The equations for designing the parameters of this bidirectional converter are presented in (22)-(29).

$$D_{Buck}=\frac{V_L}{V_H} \tag{22}$$

$$D_{Boost}=1-D_{Buck} \tag{23}$$

$$R_L=\frac{V_L^2}{P} \tag{24}$$

$$R_H=\frac{V_H^2}{P} \tag{25}$$

$$L_{Buck}=(1-D_{Buck})*R_L/2/f \tag{26}$$

$$L_{Boost}=D_{Boost}*(1-D_{Buck})*2*R_H/2/f \tag{27}$$

$$C_L=(1-D_{Boost})/8/L/K_{rh}/f^2 \tag{28}$$

$$C_H=D_{Boost}/R_L/f/K_{rl} \quad (29)$$

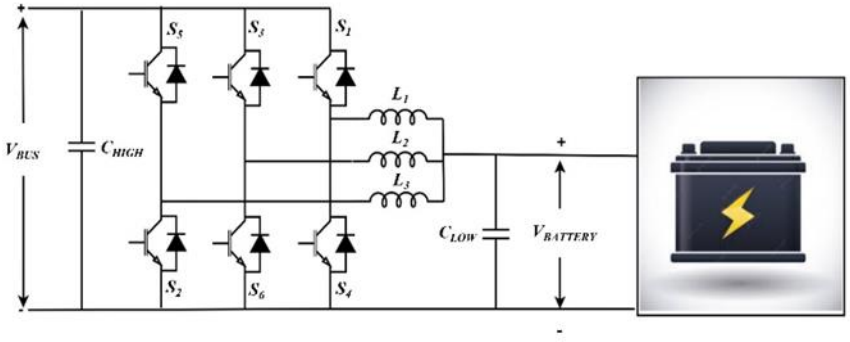

Fig. 4 Battery system with bidirectional DC-DC converter

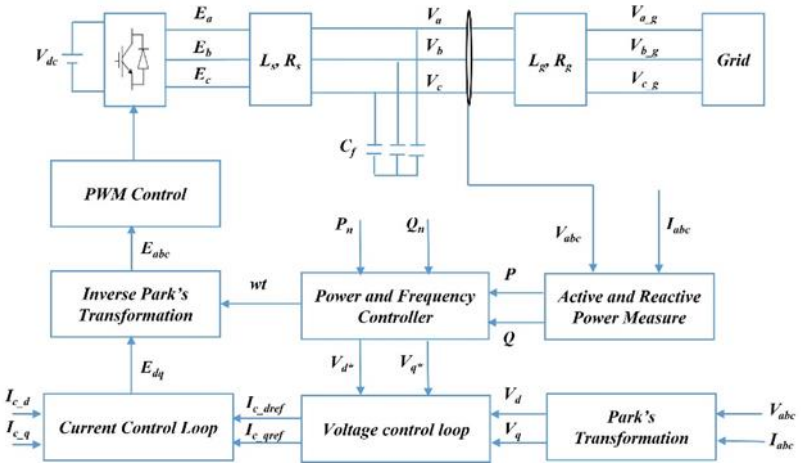

Fig. 5 VSG CONTROL

F. VSG Control Scheme

Fig. 5 illustrates the control scheme for the VSG. The primary components of the VSG include an inverter bridge, a filter, and a control system. A Capacitive filter is used to improve filtering performance. The VSG control system is based on four essential functions: active power, frequency, voltage, and voltage stability controllers [14].

Where, V_{dc} represents the DC link reference voltage, while R_s, L_s denote the line impedance at the inverter side, and R_g, L_g represent the line impedance at the grid side. The filter capacitance is indicated by C. The generator voltages are given by V_d, V_q in the d-q reference frame, while $V_{a,b,c}$ represent the load voltages, and V_{a_g} , V_{b_g} , V_{c_g} indicate the grid voltages. Additionally, the filter currents in the d-q reference frame are represented by I_{c_d}, I_{c_q}, with I_{c_dref}, I_{c_qref} denoting their respective reference current values. The reference values for active and reactive power are denoted by P_n, Q_n, respectively.

F.1 Reactive and Active Power Controller

Active and reactive power control ensures that distributed generators consistently deliver scheduled power output, utilizing both an outer power control loop and an inner current control loop. This control strategy is commonly applied in grid-connected Virtual Synchronous Generator (VSG) units. In utility-connected mode, the governor unit precisely regulates active power, following dispatch instructions closely. However, the reactive power controller struggles to follow the dispatched commands effectively, often failing to deliver the necessary reactive power to the system. The active power control in VSG mimics the governor unit of a synchronous generator (SG) [15].

F.2 Frequency and Power Controller

The power controller in Virtual Synchronous Generator (VSG) control plays a key role in replicating the dynamics of rotating synchronous generators (SGs) and helps maintain the stability of the power system. Fig. 6 presents a block diagram of the power controller, which serves as a unified mechanism, managing both the VSG's power output and the grid frequency simultaneously. To introduce inertia into the system dynamics, the inertia coefficient 'J' is integrated into the grid-connected inverter. The simple swing equation of a synchronous generator (SG) forms the core of the VSG. Equations (30) and (31) provide the power control with inertia response. The power and frequency controller enables active power regulation and ensures frequency stability within the system, while also contributing to an effective active frequency response [16].

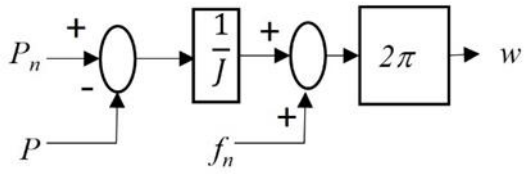

Fig. 6 Power controller

$$J\frac{dw}{dt}=T_m-T_e-T_d=T_m-T_e-D(w-w_o) \tag{30}$$

$$T_e=\frac{P_e}{w}=(e_a i_a+e_b i_b+e_c i_c)/w \tag{31}$$

III. Simulation Model

Fig. 7 depicts a HSWS equipped with an inverter controlled by a virtual synchronous generator. The system model aligns with the diagram, utilizing the parameters listed in Table 1.

Table 1. Specifications

Parameters	***Values***
No. of series strings	*4*
Number of parallel connected strings	*58*
Number of cells per Panel	*96*
Panel power rating	*75 kW*
V_{oc}	*64.2 V*
I_{sc}	*5.96 A*
Wind Turbine output power	*500 W*
$W_{cut\text{-}in\ speed}$	*3 m/s*
$W_{cut\text{-}out\ speed}$	*58 m/s*
Battery bank voltage	*144*
Inverter rated Power	*75 kVA*
Switching frequency	*1.2 mH*
Filter Inductance L	*1500 µF*
Filter Capacitance C	*182 mF*
Reference voltage Vdc	*300 V*

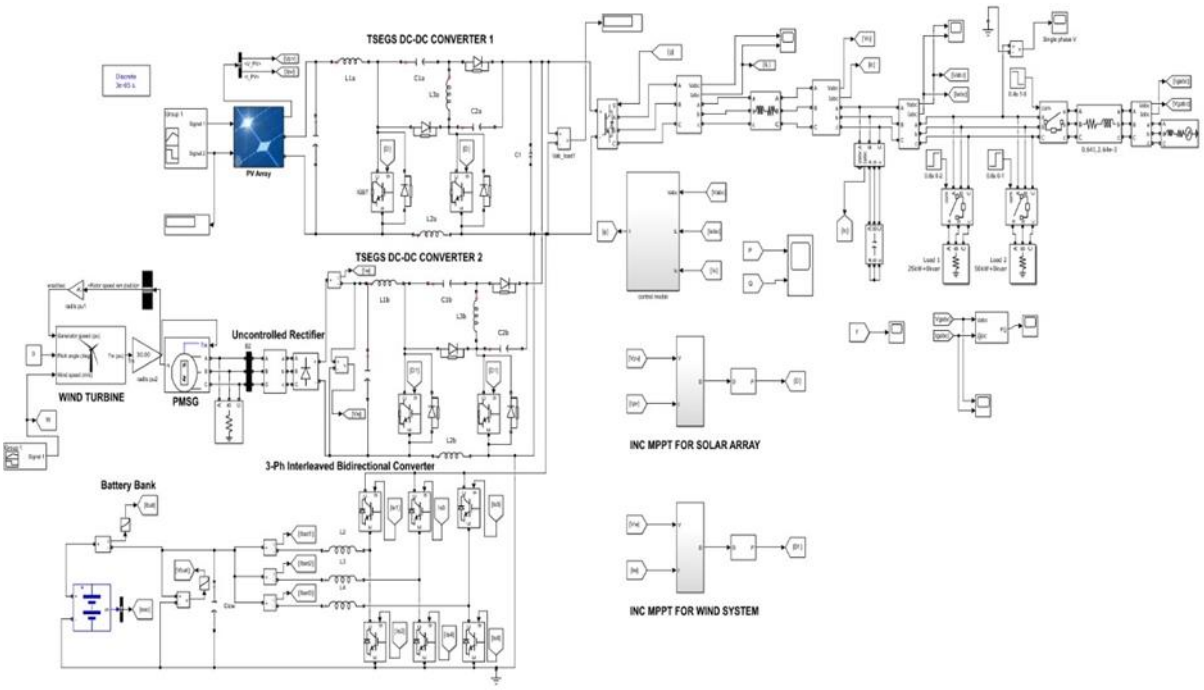

Fig. 7 Simulation Model of HSWS with VSG control

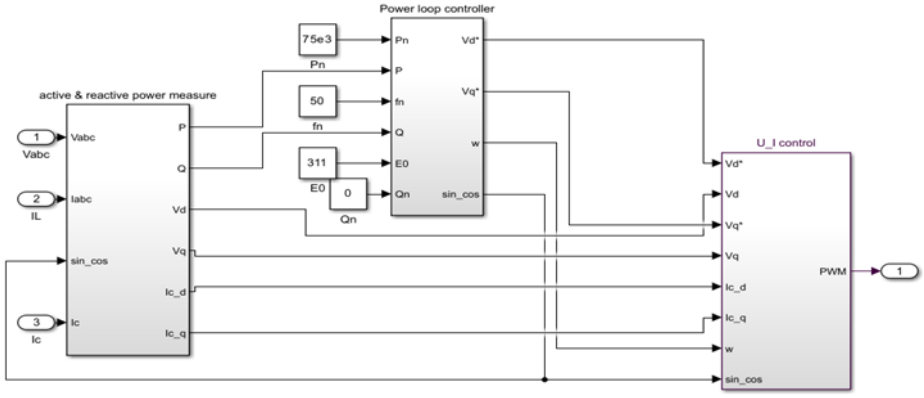

Fig. 8 VSG Control

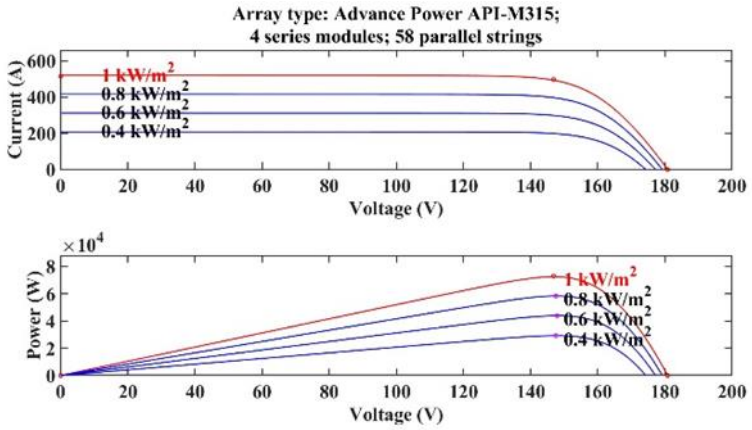

Fig. 9 PV and IV curve under different Solar radiations

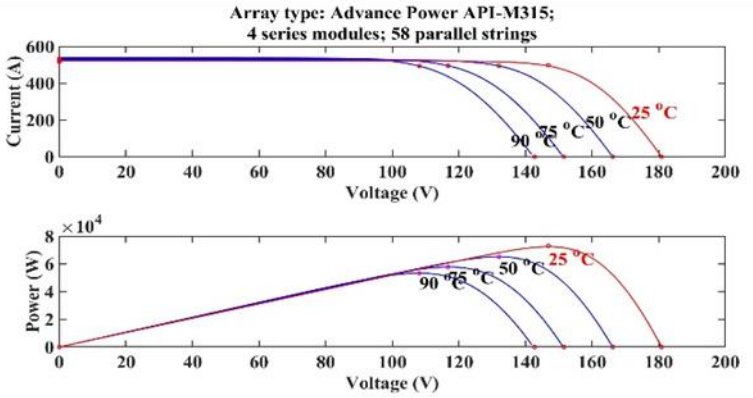

Fig. 10 PV and IV curve under different temperatures

IV. RESULTS AND DISCUSSIONS

This work presents a simulation model of a grid-connected system equipped with a VSI and its corresponding control algorithm. Fig. 9 and Fig. 10 illustrate the power-voltage (PV) and voltage-current (VI) characteristics of the solar array across different levels of solar irradiation and temperatures. The figures indicate that maximum power generation, reaching 75 kW, occurs at a solar irradiation of 1000 W/m² and a temperature of 25°C. A decrease in both solar irradiation and temperature results in a reduction in power output. Fig. 11 illustrates the relationship between wind speed and the output power of a wind turbine. The curve shows that the turbine's cut-in speed, or the minimum speed required for rotation and power generation, is 3 m/s. The rated speed, occurring at 12 m/s, corresponds to the turbine producing its maximum power of 500 watts. When the wind speed exceeds this rated level, the turbine's power output gradually declines, eventually reaching zero at a wind speed of 40 m/s. This speed, known as the cut-out speed, marks the point beyond which the turbine ceases to generate power.

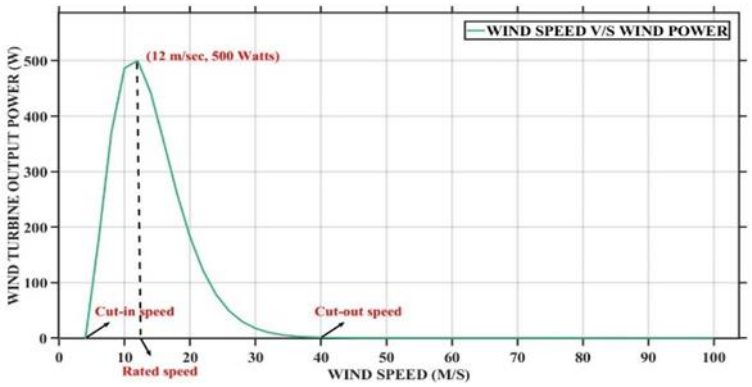

Fig. 11 Wind speed v/s wind turbine output power

Simulation initially starts with 75kW loads and the grid. After 0.4 sec the grid is disconnected and islanded but the inverter feeds both 25kW load and 50KW load. After 0.6 sec, 50KW load is disconnected and only 25kW load gets its supply from the inverter. The grid voltage remains constant during this time, but the grid current decreases to zero after 0.4 sec. When the grid is connected to the system we can see that there are little distortions in the load voltage and load current, after the grid remains in islanded mode the load voltage and current remains constant. After the grid gets disconnected after 0.4sec, the active power at the grid attains the rated power and the reactive power reduces to zero.

The Total Harmonic Distortion (THD) analysis was also conducted on the grid side, where the THD percentage for both grid current and grid voltage was measured. The results show that the grid current has a THD of 3.06%, indicating a moderate level of harmonics present in the current waveform, potentially affecting power quality. Meanwhile, the grid voltage exhibits a THD of 1.94%, suggesting relatively lower harmonic distortion in the

voltage waveform compared to the current. These values help assess the overall power quality and the extent of harmonic distortion affecting the grid system.

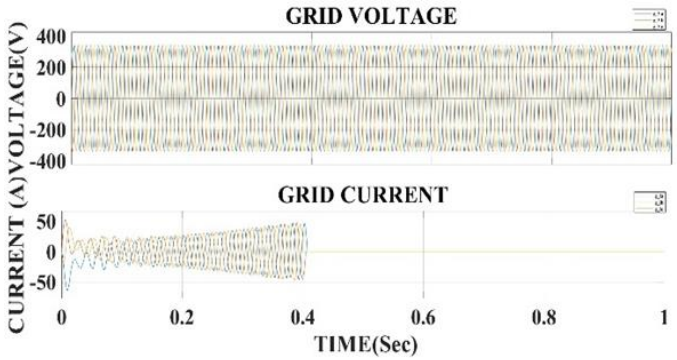

Fig. 12 Grid voltage and current

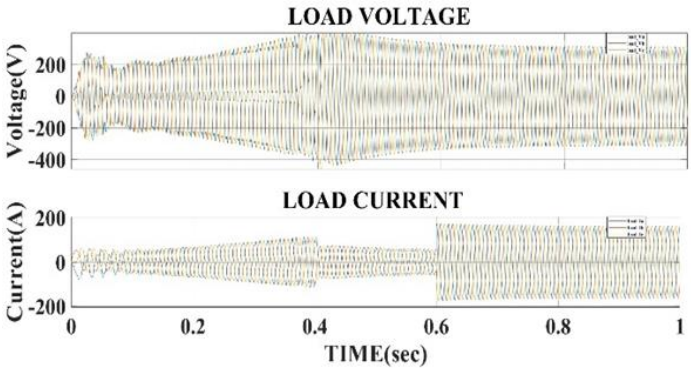

Fig. 13 Load voltage and load current

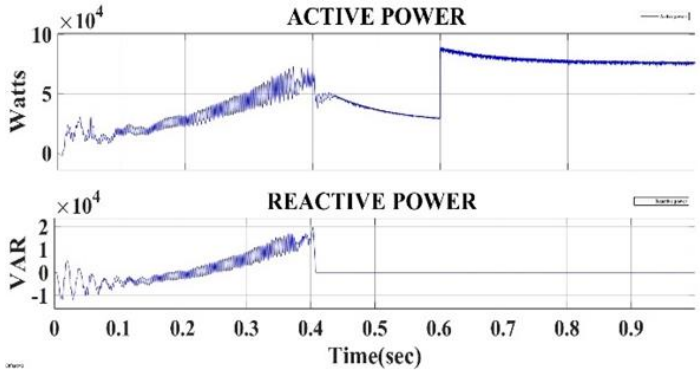

Fig. 14 Active power and reactive power

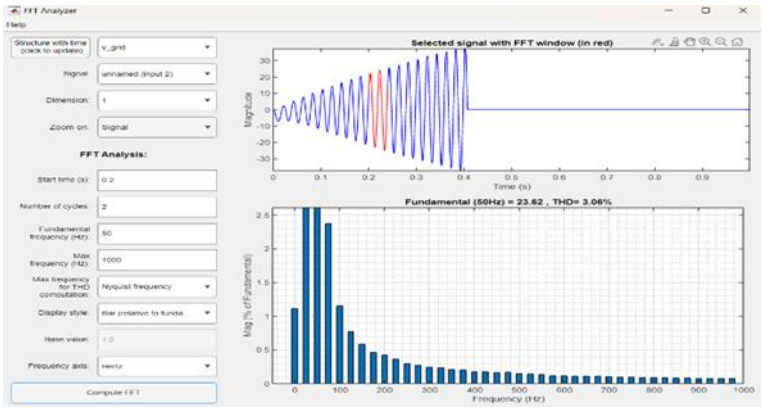

Fig. 15 THD of the grid current

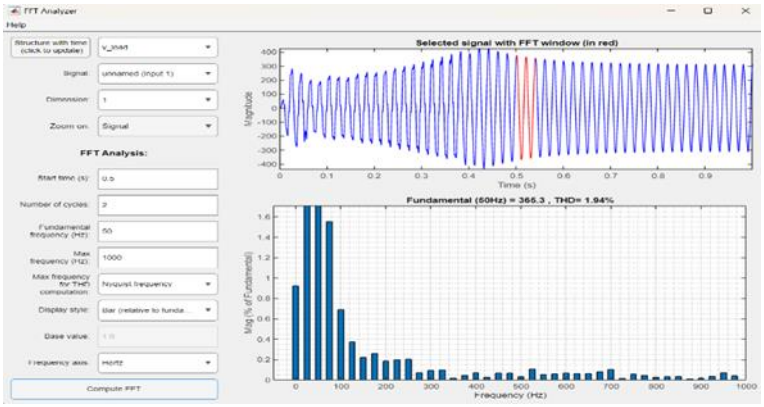

Fig. 16 THD of the grid voltage

V. CONCLUSION

In this study, a grid-connected inverter with a VSG control technique is developed for a hybrid solar-wind system, emulating the behavior of traditional synchronous generators. This enables the VSG to efficiently stabilize both voltage and frequency in the grid. From the MATLAB simulation results, it is evident that the model, with the inverter supplied by a high-gain DC-DC converter and using a PV panel and wind turbine as primary power sources, demonstrates reduced fluctuations. The Total Harmonic Distortion (THD) values for the system using the VSG-controlled inverter are as follows: grid current is 3.06%, and grid voltage is 1.94%. All these values fall below the 5% THD threshold. Hence, incorporating a VSG control algorithm into a hybrid system offers a reliable and sustainable approach to improving grid stability.

REFERENCES

[1] M. Sechilariu, B. Wang, and F. Locment, “Building integrated photovoltaic system with energy storage and smart grid communication,” IEEE Transactions on Industrial Electronics, vol. 60, no. 4, pp. 1607–1618, 2013, , https://doi.org/ 10.1109/TIE.2012.2222852.

[2] Q. Hassan, S. Algburi, A. Z. Sameen, H. M. Salman, and M. Jaszczur, “A review of hybrid renewable energy systems: Solar and wind-powered solutions: Challenges, opportunities, and policy implications,” Dec. 01, 2023, Elsevier B.V. , https://doi.org/ 10.1016/j.rineng.2023.101621.

[3] T. Arunkumari and V. Indragandhi, “An overview of high voltage conversion ratio DC-DC converter configurations used in DC micro-grid architectures,” 2017, Elsevier Ltd.

https://doi.org/ 10.1016/j.rser.2017.04.036.

[4] S. Selvam, M. Sannasy, and M. Sridharan, “Small-Signal Modeling of Two - Switch Enhanced Gain Modified SEPIC Converter,” in PESGRE 2022 - IEEE International Conference on “Power Electronics, Smart Grid, and Renewable Energy,” Institute of Electrical and Electronics Engineers Inc., 2022. , https://doi.org/10.1109/PESGRE52268.2022.9715902.

[5] M. Veerachary and M. R. Khuntia, “Analysis and Design of Two-Switch Enhanced Gain SEPIC Converter,” IEEE Transactions on Industrial Electronics, vol. 69, no. 4, pp. 3577–3587, Apr. 2022.

[6] R. B. Bollipo, S. Mikkili, and P. K. Bonthagorla, “Hybrid, optimal, intelligent and classical PV MPPT techniques: A review,” Jan. 01, 2021, Institute of Electrical and Electronics Engineers Inc. , https://doi.org/ 10.17775/CSEEJPES.2019.02720.

[7] D. C. Huynh and M. W. Dunnigan, “Development and comparison of an improved incremental conductance algorithm for tracking the MPP of a solar PV panel,” IEEE Trans Sustain Energy, vol. 7, no. 4, pp. 1421–1429, Oct. 2016, , https://doi.org/ 10.1109/TSTE.2016.2556678.

[8] H. Hasabelrasul, Z. Cai, L. Sun, X. Suo, and I. Matraji, “Two-Stage Converter Standalone PV-Battery System Based on VSG Control,” IEEE Access, vol. 10, pp. 39825–39832, 2022,

https://doi.org/10.1109/ACCESS.2022.3165664.

[9] J. Alipoor, Y. Miura, and T. Ise, “Power system stabilization using virtual synchronous generator with alternating moment of inertia,” IEEE J Emerg Sel Top Power Electron, vol. 3, no. 2, pp. 451–458, Jun. 2015, https://doi.org/ 10.1109/JESTPE.2014.2362530.

[10] H. Parveen and A. R. Ram, “A PSO-ANFIS MPPT-Based 3-Phase Series Resonant Converter with DLLC Tanks for Hybrid Solar Wind Battery System with DC-Load,” SSRG International Journal of Electrical and Electronics Engineering, vol. 10, no. 7, pp. 199–210, Jul. 2023, https://doi.org/ 10.14445/23488379/IJEEE-V10I7P118.

[11] F. Wang, Y. Wang, B. Su, and C. Teng, “Three-phase interleaved high step-up bidirectional DC-DC converter,” IET Power Electronics, vol. 13, no. 12, pp. 2638–2650, Sep. 2020, https://doi.org/10.1049/iet-pel.2020.0295.

[12] H. Parveen, Dr. A. Raghu Ram “Design and Performance Analysis of SEPIC Converter With Different MPPT Control Algorithms For Hybrid Solar-Wind System,” NeuroQuantology, vol. 20, no. 19, pp. 2391-2400, Dec. 2022, https://doi.org/10.48047/nq.2022.20.19.NQ99201

[13] H. Parveen and A. R. Ram, "An Artificial Intelligence-Based Hybrid MPPT Technique for SEPIC Converter Applied to Hybrid Renewable Energy Systems with Battery Storage," 2023 10th IEEE Uttar Pradesh Section International Conference on Electrical, Electronics and Computer Engineering (UPCON), Gautam Buddha Nagar, India, 2023, pp. 1026-1031, , https://doi.org/10.1109/UPCON59197.2023.10434729.

[14] H. Hasabelrasul, Z. Cai, L. Sun, X. Suo, and I. Matraji, “Two-Stage Converter Standalone PV-Battery System Based on VSG Control,” IEEE Access, vol. 10, pp. 39825–39832, 2022, https://doi.org/10.1109/ACCESS.2022.3165664

[15] M. Chen, D. Zhou, and F. Blaabjerg, “Modelling, Implementation, and Assessment of Virtual Synchronous Generator in Power Systems,” Journal of Modern Power Systems and Clean Energy, vol. 8, no. 3, pp. 399–411, May 2020, https://doi.org/10.35833/MPCE.2019.000592.

[16] M. S. Haritha and D. S. Nair, "Review on virtual synchronous generator (VSG) for enhancing performance of microgrid," 2018 International Conference on Power, Signals, Control and Computation (EPSCICON), Thrissur, India, 2018, pp. 1-5, https://doi.org/10.1109/EPSCICON.2018.8379587.